ChemComm

COMMUNICATION

View Article Online
View Journal | View Issue

Cite this: *Chem. Commun.*, 2026, 62, 9749

Received 3rd March 2026,
Accepted 15th April 2026

DOI: 10.1039/d6cc01294a

rsc.li/chemcomm

Ligand rigidity as a design principle for planar pentacoordinate fluorine

Li-Xia Bai,[a] Ya-Xuan Cheng,[a] Fernando Martínez-Villarino,[b] Luz Diego,[c] Jin-Chang Guo *[a] and Gabriel Merino *[b]

Planar hypercoordinate fluorine is rare due to the high electronegativity of F. A Zn_5O_5 framework stabilizes D_{5h} F©$Zn_5O_5^-$ as a global minimum. The bonding is predominantly electrostatic with a minor covalent contribution. A detachment energy of 6.29 eV places the cluster in the superhalogen regime.

Planar hypercoordinate atoms challenge the relationship between coordination number, geometry, and bonding. The field originated from the concept of planar tetracoordinate carbon (ptC), proposed by Monkhorst in 1968 as a hypothetical transition-state structure.[1] Subsequent theoretical studies by Hoffmann, Alder, and Wilcox established the electronic requirements for stabilizing ptC transition states, showing that while specific bonding patterns can reduce the energetic penalty relative to tetrahedral carbon, the planar form remains intrinsically higher in energy.[2] Based on these principles, Schleyer and co-workers predicted the first viable ptC molecule, 1,1-dilithiocyclopropane.[3] Since then, numerous ptC species have been proposed and experimentally characterized,[4] including several aluminum-based ptC clusters detected by gas-phase photoelectron spectroscopy.[5–8]

Following the establishment of ptC, efforts focused on increasing the coordination number while preserving planarity. A key milestone was the prediction of the first planar pentacoordinate carbon (ppC) global minimum, C©Al_5^+,[9] which adopts D_{5h} symmetry. This example was followed by theoretical studies showing that, while ppC motifs can be stabilized through diverse electronic and structural strategies,[10] further increases in coordination number impose stronger structural and electronic constraints. For instance, the C©B_6^{2-} wheel corresponds to a local minimum rather than a global minimum.[11] To address these limitations, alternative bonding strategies were explored. Using a mixed electrostatic-covalent approach, planar hexacoordinate carbon (phC) clusters of the type C©$E_3M_3^+$ (E = S–Te, M = Li–Cs) were designed.[12] These systems show that combining electrostatic stabilization with multicenter interactions provides a route to high planar coordination in carbon-centered clusters.

Advances in carbon-centered systems stimulated the exploration of planar tetracoordination in other p-block elements.[13] Predictions extended to B,[14] N,[15] and O,[16] followed by studies confirming the existence of planar tetracoordinate Si and Ge species, $SiAl_4^-$ and $GeAl_4^-$.[17] In these systems, multicenter π and σ bonding plays a central role in stabilizing planar geometries. Beyond tetracoordination, planar hypercoordinate p-block clusters have also been reported, including planar pentacoordinate B,[18] N,[19] O,[20] S,[21] Se,[22] as well as planar hexacoordinate Si.[23]

Planar hypercoordinate s-block atoms rely on electron delocalization enabled by vacant p orbitals rather than conventional covalent bonding. Examples include planar pentacoordinate lithium Li©Na_5 and planar pentacoordinate beryllium Be©M_5^+ (M = Cu, Ag).[24,25] Hydrogen can also adopt planar hypercoordinate environments. Planar tetracoordinate and pentacoordinate hydrogen clusters have been reported, including H©In_4^+,[26] H©$K_4H_4^-$,[27] H©$Li_5H_5^-$,[28] and H©$Cu_5H_5^-$.[29] Recent studies have extended the limits of planar hypercoordination. Using honorary transition-metals, coordination numbers up to fifteen have been reported for planar alkaline-earth metal centers.[30] For comparison, the highest coordination number reported for a planar transition-metal system is ten.[31]

Fluorine is among the most challenging elements for planar hypercoordination. Its high electronegativity promotes localization of valence electrons as lone pairs, limiting participation in delocalized bonding. Early planar tetracoordinate fluorine (ptF) clusters, such as F©In_4^+ and F©Tl_4^+, were identified as global minima at the DFT level.[32] At the CCSD(T) level with large basis sets, slight contraction of the ligand ring induces a small out-of-plane displacement of the F atom, converting these structures into transition states.[33] However, the associated energy

[a] *Institute of Molecular Science, Shanxi University, Taiyuan 030006, China. E-mail: guojc@sxu.edu.cn*

[b] *Departamento de Física Aplicada, Centro de Investigación y de Estudios Avanzados, Unidad Mérida. Km 6 Antigua Carretera a Progreso. Apdo. Postal 73, Cordemex, 97310, Mérida, Yucatan, México. E-mail: gmerino@cinvestav.mx*

[c] *Doctorado en Fisicoquímica Molecular, Facultad de Ciencias Exactas, Universidad Andres Bello, Av. República 275, Santiago, Chile*

differences are small, and the structural distortion remains minimal, indicating a shallow potential energy surface (PES) and an effectively planar geometry. More recently, additional ptF global minima have been reported, including $F©Li_4H_3^-$,[34] $F©K_4H_4^-$,[35] $F©Mg_4Se_4^-$,[36] $F©Li_4M_4^-$ (M = Ag, Au),[37] and $F©Li_4F_3^-$.[38] In these clusters, ligand rings composed of alkali or alkaline-earth metals, often assisted with bridging atoms, provide an electrostatic environment that stabilizes a planar F center.

Recently, the star-like $F©Li_5F_5^-$ cluster was reported as the first planar pentacoordinate fluorine (ppF) global minimum.[39] However, this structure is only marginally more stable than the corresponding ptF isomer, with an energy difference of approximately 0.2 kcal mol^{-1}. This small energy gap indicates that the ligand framework does not provide a stable structural platform, allowing interconversion between coordination motifs and limiting stabilization of the ppF arrangement. In such core–shell architectures, where the interaction between F and the ligand framework is predominantly electrostatic, the intrinsic stability of the ring becomes a key factor for achieving higher coordination numbers.

The hollow Li_5F_5 ring does not correspond to a global minimum and lies 9.3 kcal mol^{-1} above its lowest-energy form at the PBE0-D3(BJ)/def2-TZVPP level. In contrast, the $O©Be_5O_5^{2-}$ dianion, which contains a ppO atom, is supported by a Be_5O_5 ring that is itself a stable structural motif. In this system, the Be–O interactions exhibit a larger covalent contribution, stabilizing the ligand framework.

Zn-group elements share bonding features with alkaline-earth metals, particularly in their interactions with O. Based on this analogy, Zn-group atoms were considered as ligands, with O atoms acting as bridging units to stabilize a ppF center. From an orbital perspective, the LUMO of the Zn_5O_5 ring is localized at the center of the cavity (Fig. S1), indicating that this region can accommodate additional electron density and provide a favorable site for the F atom. Together, these considerations point to Zn_5O_5 as a suitable framework for stabilizing a ppF center.

To examine this design principle, a series of forty $FM_5X_5^-$ clusters was evaluated, where M = Be–Ba, Zn–Hg and X = O–Po. At the PBE0-D3(BJ)/def2-TZVPP level, most tested structures show a mismatch between the size of the F atom and that of the ligand cavity, reflected in their vibrational profiles, which exhibit multiple imaginary frequencies (N_{IMG} = 4–10) with magnitudes of 100–300i cm^{-1} (Table S1).

Within this series, only $F©Zn_5O_5^-$ (**1**) corresponds to a true minimum on the PES (Fig. 1). The Zn_5O_5 ring is a known global minimum with D_{5h} symmetry, as reported by Woodley *et al.*,[40] and provides a geometrically compatible framework that accommodates the central F atom (Fig. 1). Wiberg bond indices (WBI) further indicate a larger degree of covalent interaction within the Zn_5O_5 ring (WBI_{Zn-O} = 0.54) compared to the Li_5F_5 framework (WBI_{Li-F} = 0.09; Fig. S2), supporting the stability of this ligand motif.

Vibrational frequency analyses of **1** were performed at multiple theoretical levels. As shown in Table S2, the lowest vibrational frequencies lie in the range of 47 to 54 cm^{-1}, confirming **1** as a true minimum rather than a method-dependent artifact.

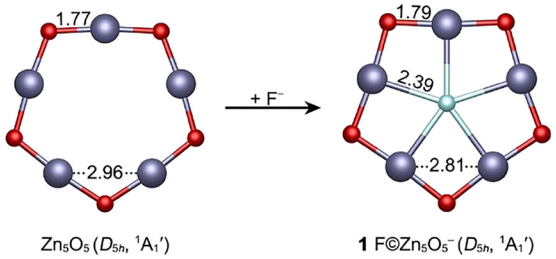

Fig. 1 PBE0-D3(BJ)/def2-TZVPP geometries of Zn_5O_5 and $F©Zn_5O_5^-$. The bond distances are in Å.

The stability of this structure is supported by comparison with low-lying isomers (Fig. S3). Structure **1** lies 11.4 kcal mol^{-1} below the second-lowest isomer, **2**, obtained by interchanging the F atom with one of the bridging O atoms. Among these isomers, structures **1–3** are planar, whereas isomers **4–8** adopt 3D geometries. A clear energetic separation is also found between spin states, with the lowest triplet isomer lying 72.6 kcal mol^{-1} above the global minimum. A ptF isomer analogous to that reported for $Li_5F_6^-$ was also constructed; upon optimization, it relaxes directly to **1**.

Geometrically, the Zn–F distance in **1** is 2.39 Å, which is longer than the covalent single-bond distance of 1.82 Å proposed by Pyykkö.[41] The low WBI_{Zn-F} value of 0.07 indicates weakly covalent Zn–F interactions (Fig. S4). In contrast, the Zn–O bond length of 1.79 Å and the corresponding WBI_{Zn-O} of 0.53 show a larger covalent contribution within the Zn_5O_5 ring. The Zn–Zn separations of 2.81 Å exceed typical covalent bond lengths (2.36 Å) and exhibit negligible bond indices, ruling out direct Zn–Zn bonding. In the isolated Zn_5O_5 ring, the Zn–Zn distance is longer (2.96 Å) and the Zn–O bond length is shorter (1.77 Å). Upon incorporation of a central F atom, the Zn_5O_5 ring contracts, as reflected in shorter Zn–Zn distances and slightly elongated Zn–O bonds, indicating a structural reorganization of the ligand framework.

Natural population analysis indicates a polarized charge distribution within the cluster. In **1**, the F atom carries a charge of −0.85 $|e|$, while the O atoms and Zn centers bear charges of about −1.36 and +1.33 $|e|$, respectively. The charge on F is less negative than that of an isolated F^- anion, indicating partial depletion of electron density upon coordination. Comparison with the isolated Zn_5O_5 ring (Zn +1.35 $|e|$, O −1.35 $|e|$) shows only minor changes within the ligand framework. So, the stabilization of the ppF structure is associated with a reduction in charge localization upon F coordination, resulting in a more distributed charge within the cluster.

The electron density analysis also reveals distinct interaction regimes for Zn–F and Zn–O contacts (Table S3). Bond critical points (BCP) and associated gradient paths between F and Zn atoms, confirm the planar pentacoordinate arrangement around F (Fig. S5). The Zn–F interactions show low electron density ($\rho(\mathbf{r})$ = 0.029), positive Laplacians ($\nabla^2\rho(\mathbf{r})$ = 0.122), slightly positive energy densities ($H(\mathbf{r})$ = 0.0004), and a $-G(\mathbf{r})/V(\mathbf{r})$ ratio close to unity (1.014), indicating closed-shell interactions. The delocalization index is small (DI = 0.15), indicating limited

electron sharing. In contrast, the Zn–O interactions display higher electron density at the BCP ($\rho(\mathbf{r})$ = 0.134), negative energy densities ($H(\mathbf{r})$ = −0.048), and a $-G(\mathbf{r})/V(\mathbf{r})$ ratio of 0.81, and a larger delocalization index (DI = 0.83), evidencing greater electron sharing between Zn and O atoms.

Interatomic interaction energies from interacting quantum atoms (IQA) analysis (Table S4) show that both Zn–F and Zn–O interactions are dominated by electrostatic contributions, whereas Zn–Zn interactions are repulsive, reflecting the charge distribution. For Zn–F contacts, the electrostatic term accounts for 88.1% of the interaction energy, with an exchange–correlation contribution of 11.9%, indicating a limited covalent character. In contrast, Zn–O interactions are stronger and show a larger exchange–correlation component (ca. 30%), while remaining predominantly electrostatic.

AdNDP is used to characterize the bonding pattern of the Zn_5O_5 framework and to evaluate whether the F atom participates in delocalized bonding or remains largely localized. The AdNDP results show that each Zn atom accommodates five lone pairs, the F atom carries four lone pairs (arising from its high electronegativity), and each O atom contributes one localized lone pair (Fig. 2). The Zn_5O_5 framework is stabilized by ten localized 2c–2e Zn–O σ bonds and five 3c–2e Zn–O–Zn π bonds. The MOs associated with the 3c–2e π bonds (HOMO, HOMO−1, and HOMO−4, Table S5) are dominated by O contributions (84–87%), with smaller but non-negligible participation from Zn (12–16%).

When the 3c–2e π bonds are localized as O lone pairs, the ONs decrease to 1.91 $|e|$ (Fig. S6). Concomitantly, the electron pair initially assigned as a F–centered 2s lone pair can be alternatively described as a 6c–2e σ interaction involving the Zn d orbitals. In this representation, the ON increases from 1.96 to 2.00 $|e|$. Both representations correspond to different partitions of the same electron density and provide an equivalent description of the bonding. In this sense, the molecule is indifferent to the chosen representation, provided that the underlying electronic structure is properly described. Nevertheless, the multicenter description is preferred, as it preserves the optimal ONs and aligns with the Mulliken orbital analysis (Table S5), which indicates a dominant O contribution with secondary participation from Zn.

EDA–NOCV provides a complementary description of the bonding. The optimal fragmentation scheme, defined by the smallest orbital interaction term (ΔE_{oi}), corresponds to interaction between a singlet F^- fragment and a singlet neutral Zn_5O_5 unit. Results obtained using alternative fragmentation schemes are provided in Table S6. Electrostatic interactions (ΔV_{elstat}) account for 71.7% of the total attractive energy, while orbital interactions contribute 28.3% (Table S7). The dominant orbital contributions arise from $\Delta E_{oi(1)-(3)}$, corresponding to σ donation from the F 2s → Zn_5O_5 and two degenerate dative bonds involving the F($2p_x$/$2p_y$) orbitals (Table S7). The corresponding deformation densities ($\Delta\rho$) are depicted in Fig. 3.

So, the overall negative–positive–negative arrangement from the center to the periphery show dominant electrostatic interactions within the system, and the cluster can be described as $[F]^-[Zn_5O_5]$. The formation of F©$Zn_5O_5^-$ from Zn_5O_5 and F^- is exothermic (−106.4 kcal mol^{-1} at the PBE0-D3(BJ)/def2-TZVPP level including zero-point corrections), indicating a thermodynamically favorable process.

The symmetry of **1** may suggest aromatic stabilization from a geometric perspective. However, magnetic response analyses do not support this interpretation. The B_z^{ind} displays a localized shielding cone centered on the F atom, ruling out delocalized ring currents (Fig. 4). Accordingly, the induced current density ($\mathbf{J}^{ind}$) does not show a continuous diatropic current circulating around the framework but remains localized around individual atoms. A small diatropic contribution near F correlates with the shielding cone and can be attributed to the localized lone pair on this atom. So, both magnetic descriptors indicate that **1** does not exhibit global aromatic behavior and that its magnetic response is dominated by local contributions.

The electronic stability of F©$Zn_5O_5^-$ was evaluated through analysis of its frontier MOs. The HOMO–LUMO gap of 5.56 eV indicates a robust electronic structure (Fig. S7). Electron attachment is unfavorable, as reflected by the positive LUMO energy of 1.99 eV. Consistently, the neutral F©Zn_5O_5 system corresponds to a saddle point with one imaginary frequency, while the dianion exhibits four imaginary frequencies, indicating that both electron attachment and electron detachment destabilize

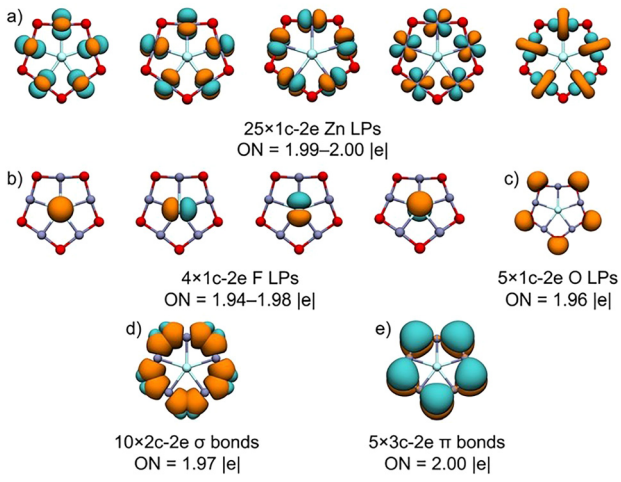

Fig. 2 AdNDP bonding pattern of F©$Zn_5O_5^-$ at the PBE0/def2-TZVPP level. Occupation numbers (ONs, in $|e|$) are indicated. (a) Twenty-five lone pairs (LPs) localized on the Zn atoms; (b) four LPs on the F atom; (c) five LPs on the O atoms; (d) ten 2c–2e Zn–O σ bonds; (e) five 3c–2e Zn–O–Zn π bonds.

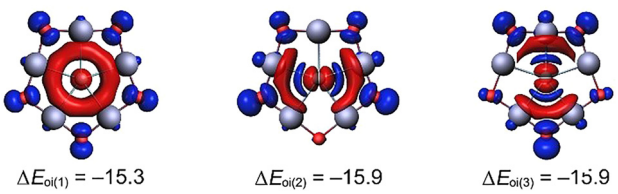

Fig. 3 The deformation densities ($\Delta\rho$) obtained *via* EDA–NOCV analysis. The isovalues of the surfaces are 0.0008 for $\Delta\rho_{oi(1)}$ and 0.0005 for $\Delta\rho_{oi(2)-(3)}$. The direction of charge flow is from red to blue. Energy values are given in kcal mol^{-1}.

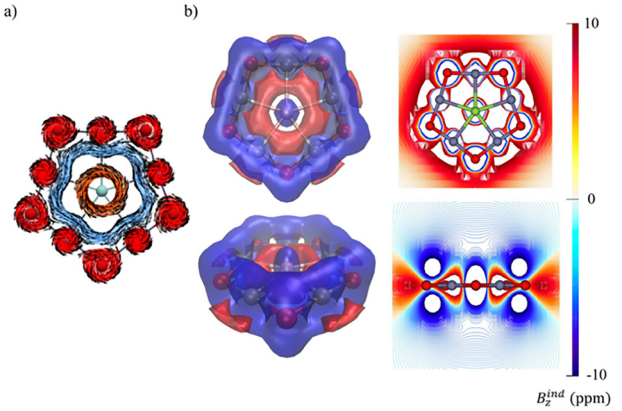

Fig. 4 (a) Magnetically induced current density $\mathbf{J}^{ind}$ maps for F©$Zn_5O_5^-$. Arrows indicate the direction of the current density. (b) B_z^{ind} isolines plotted in the molecular plane (bottom) and a transverse plane (top) of the F©$Zn_5O_5^-$. The external magnetic field is oriented perpendicular to the molecular plane.

the system. Superhalogen anions are defined as species with vertical detachment energies exceeding the electron affinity of chlorine (3.61 eV). Several prototypical superhalogen families and planar hypercoordinate superhalogens have been reported.[42] In this context, the calculated ground-state vertical detachment energy of F©$Zn_5O_5^-$ is 6.29 eV at the CCSD(T) level, exceeding the electron affinity of chlorine and placing this system in the superhalogen regime.

Finally, dynamic stability was examined using Born–Oppenheimer molecular dynamics simulations at 300, 600, and 900 K (Fig. S8). Over 50 ps, structure **1** remains intact, with average root-mean-square deviations (RMSDs) in the range of 0.20–0.33 Å and no isomerization or fragmentation. Occasional increases in the RMSD arise from out-of-plane vibrational motion of the F atom and do not indicate structural instability.

In summary, a ppF global minimum is identified using a Zn_5O_5 ligand framework. Exploration of related $FM_5X_5^-$ compositions shows that stabilization of ppF requires the simultaneous fulfillment of several conditions: (i) the ligand ring must be a stable structural motif, preferably a global minimum on its own PES; (ii) the size of the ligand cavity must be geometrically compatible with the central atom; and (iii) the ligand framework must be electronically robust, such that incorporation of the central atom induces only minor redistribution of electron density. The Zn_5O_5 ring satisfies these conditions, providing a framework that supports a ppF center. Bonding analyses indicate that the interaction between F and the surrounding Zn atoms is predominantly electrostatic, while the Zn_5O_5 ring retains its electronic structure upon coordination. The stabilization of the ppF center is therefore associated with a reduction in charge localization rather than a significant charge transfer. The large HOMO–LUMO gap and the high vertical detachment energy further indicate that F©$Zn_5O_5^-$ is electronically stable and belongs to the superhalogen regime. This work supports a design principle for planar hypercoordinate atom species based on the stability, geometric compatibility, and electronic robustness of the ligand framework.

Conflicts of interest

There are no conflicts to declare.

Data availability

The data underlying this study are available in the manuscript and its supplementary information (SI). The supplementary information contains vibrational frequency analyses for $FM_5X_5^-$ clusters, additional frequency calculations at multiple levels, IQA energy decomposition data, electron density descriptors, EDA–NOCV results, MO composition analyses, vertical detachment energies, geometries and relative energies of low-lying isomers, Born–Oppenheimer molecular dynamics simulations, and Cartesian coordinates of reported structures. See DOI: https://doi.org/10.1039/d6cc01294a.

References

1 H. J. Monkhorst, *Chem. Commun.*, 1968, 1111–1112.
2 R. Hoffmann, R. W. Alder and C. F. Wilcox Jr., *J. Am. Chem. Soc.*, 1970, **92**, 4992–4993.
3 J. B. Collins, J. D. Dill, E. D. Jemmis, Y. Apeloig, P. V. R. Schleyer, R. Seeger and J. A. Pople, *J. Am. Chem. Soc.*, 1976, **98**, 5419–5427.
4 G. Merino, M. A. Méndez-Rojas, A. Vela and T. Heine, *J. Comput. Chem.*, 2007, **28**, 362–372.
5 X. Li, L.-S. Wang, A. I. Boldyrev and J. Simons, *J. Am. Chem. Soc.*, 1999, **121**, 6033–6038.
6 X. Li, H. F. Zhang, L. S. Wang, G. D. Geske and A. I. Boldyrev, *Angew. Chem., Int. Ed.*, 2000, **39**, 3630–3632.
7 L. S. Wang, A. I. Boldyrev, X. Li and J. Simons, *J. Am. Chem. Soc.*, 2000, **122**, 7681–7687.
8 C. J. Zhang, W. S. Dai, H. G. Xu, X. L. Xu and W. J. Zheng, *J. Phys. Chem. A*, 2022, **126**, 5621–5631.
9 Y. Pei, W. An, K. Ito, P. V. R. Schleyer and X. C. Zeng, *J. Am. Chem. Soc.*, 2008, **130**, 10394–10400.
10 V. Vassilev-Galindo, S. Pan, K. J. Donald and G. Merino, *Nat. Rev. Chem.*, 2018, **2**, 0114.
11 B. B. Averkiev, D. Y. Zubarev, L.-M. Wang, W. Huang, L.-S. Wang and A. I. Boldyrev, *J. Am. Chem. Soc.*, 2008, **130**, 9248–9250.
12 L. Leyva-Parra, L. Diego, O. Yañez, D. Inostroza, J. Barroso, A. Vásquez-Espinal, G. Merino and W. Tiznado, *Angew. Chem., Int. Ed.*, 2021, **60**, 8700–8704.
13 L. M. Yang, E. Ganz, Z. Chen, Z. X. Wang and P. V. R. Schleyer, *Angew. Chem., Int. Ed.*, 2015, **54**, 9468–9501.
14 M. Menzel, D. Steiner, H. J. Winkler, D. Schweikart, S. Mehle, S. Fau, G. Frenking, W. Massa and A. Berndt, *Angew. Chem., Int. Ed. Engl.*, 1995, **34**, 327–329.
15 R. Sun, C. Yuan, H. J. Zhai and Y. B. Wu, *J. Chem. Phys*, 2023, **158**, 144301.
16 G. Castillo-Toraya, F. Ortíz-Chi, J. Barroso, M. Orozco-Ic, L. Leyva-Parra and G. Merino, *Angew. Chem., Int. Ed.*, 2025, **64**, e202500292.
17 A. I. Boldyrev, X. Li and L. S. Wang, *Angew. Chem., Int. Ed.*, 2000, **39**, 3307–3310.
18 H. L. Yu, R. L. Sang and Y. Y. Wu, *J. Phys. Chem. A*, 2009, **113**, 3382–3386.
19 A. J. Kalita, S. S. Rohman, C. Kashyap, S. S. Ullah, I. Baruah and A. K. Guha, *Inorg. Chem.*, 2020, **59**, 17880–17883.
20 R. Sun, Y. Yang, X. Wu, H.-J. Zhai, C. Yuan and Y.-B. Wu, *Chem. Sci.*, 2025, **16**, 12873–12878.
21 P. J. Thakuria, K. Sarmah, S. K. Purkayastha, A. Das and A. K. Guha, *Chem. Commun.*, 2025, **61**, 11995–11997.
22 L. Diego, A. Vásquez-Espinal, R. Islas and G. Merino, *Chem. – Eur. J.*, 2025, **31**, e02525.
23 C. Chen, M. H. Wang, L. Y. Feng, L. Q. Zhao, J. C. Guo, H. J. Zhai, Z. H. Cui, S. Pan and G. Merino, *Chem. Sci.*, 2022, **13**, 8045–8051.
24 M. H. Wang, A. J. Kalita, M. Orozco-Ic, G. R. Yan, C. Chen, B. Yan, G. Castillo-Toraya, W. Tiznado, A. K. Guha and S. Pan, *Chem. Sci.*, 2023, **14**, 8785–8791.

25 C. Chen, Y. Q. Liu and Z. H. Cui, *Inorg. Chem.*, 2021, **60**, 16053–16058.
26 A. J. Kalita, S. S. Rohman, P. P. Sahu and A. K. Guha, *Angew. Chem., Int. Ed.*, 2024, **63**, e202317312.
27 L. X. Bai, Y. X. Jin and J. C. Guo, *Chem. Commun.*, 2024, **60**, 6300–6303.
28 K. Sarmah, A. J. Kalita, S. K. Purkayastha and A. K. Guha, *Angew. Chem., Int. Ed.*, 2024, **63**, e202318741.
29 L. X. Bai, Y. X. Jin, M. Orozco-Ic, G. Merino and J. C. Guo, *Chem. Commun.*, 2024, **60**, 14996–14999.
30 X.-B. Liu, W. Tiznado, L. J. Cui, J. Barroso, L. Leyva-Parra, L. H. Miao, H. Y. Zhang, S. Pan, G. Merino and Z. H. Cui, *J. Am. Chem. Soc.*, 2024, **146**, 16689–16697.
31 C. Romanescu, T. R. Galeev, W. L. Li, A. I. Boldyrev and L. S. Wang, *Acc. Chem. Res.*, 2013, **46**, 350–358.
32 G. Castillo-Toraya, M. Orozco-Ic, E. Dzib, X. Zarate, F. Ortíz-Chi, Z. H. Cui, J. Barroso and G. Merino, *Chem. Sci.*, 2021, **12**, 6699–6704.
33 J. Kim, E. Park, J. Park, J. Kim, W. Seo, D. Oh, J. Lee and T. K. Kim, *J. Phys. Chem. A*, 2023, **127**, 5815–5822.
34 K. Sarmah, A. J. Kalita and A. K. Guha, *Phys. Chem. Chem. Phys.*, 2024, **26**, 6678–6682.
35 Y. X. Jin, L. X. Bai and J. C. Guo, *Inorg. Chem.*, 2024, **63**, 19949–19955.
36 R. Sun, C. Yuan and Y. B. Wu, *Phys. Chem. Chem. Phys.*, 2025, **27**, 6718–6723.
37 M. Yan, L. Y. Feng, C. Q. Miao, Y. J. Wang and B. Jin, *J. Phys. Chem. A*, 2025, **129**, 4523–4528.
38 B. Jin, M. Yan, L. Y. Feng, Z. R. Wang, C. Q. Miao and Y. J. Wang, *J. Chem. Phys.*, 2025, **162**, 164301.
39 L. J. Cui, L. H. Miao, M. Orozco-Ic, L. Li, S. Pan, G. Merino and Z. H. Cui, *Angew. Chem., Int. Ed.*, 2025, **64**, e202416057.
40 C. R. A. Catlow, S. T. Bromley, S. Hamad, M. Mora-Fonz, A. A. Sokol and S. M. Woodley, *Phys. Chem. Chem. Phys.*, 2010, **12**, 786–811.
41 P. Pyykkö and M. Atsumi, *Chem. – Eur. J.*, 2009, **15**, 186–197.
42 G. L. Gutsev and A. I. Boldyrev, *Chem. Phys.*, 1981, **56**, 277–283.